Lasers in Manufacturing Conference 2025

Enhancing layer adhesion in material extrusion AM with adaptive laser preheating integrated in printhead

Meisner, Dennis[a]; Kaftiranis, Nikitas[a]; Maiwald, Frederik[a]; Rapp, Petra[b]; Hierl, Stefan[a]

[a] *Laser Material Processing Laboratory, Ostbayerische Technische Hochschule Regensburg, Am Campus 1, 92331 Parsberg, Germany*
[b] *Multec GmbH, Spitzäcker 2, 88682 Salem, Germany*

Abstract

Material extrusion is a widely used additive manufacturing (AM) process that is gaining industrial acceptance due to its material variety, flexibility, and relatively low invest. However, its application is limited by process-related anisotropy, caused by insufficient interlayer bonding due to insufficient temperature in the deposition area. To improve this, an adaptive laser preheating system is added to a conventional printhead. The setup includes eight separately controlled, fiber-coupled diode lasers arranged concentrically around the nozzle. This enables various intensity distributions and thus direction-dependent heating.
This work investigates the effect of three laser intensity profiles — spot, sickle, and ring — on interlayer bonding under varying cooling conditions. Laser preheating improves tensile strength in build direction up to approx. 40 %, with the ring-shaped distribution delivering the highest strength. This demonstrates the potential of laser preheating to significantly reduce anisotropy in extrusion-based AM.
However, the additional energy must be well balanced: improper thermal management can reverse the benefits of preheating and degrade mechanical properties.

Keywords material extrusion AM; fused layer modeling; laser preheating; anisotropy; interlayer bonding

1. Introduction

Additive manufacturing (AM) via extrusion-based processes — commonly referred to as Fused Layer Modeling (FLM), Fused Filament Fabrication (FFF), or Fused Deposition Modeling (FDM) — offers significant advantages due to its broad material variety, design flexibility, and relatively low investment costs [1]. These characteristics have enabled a wide range of industrial applications, particularly in prototyping and small-batch production.

A key limitation of FLM is its pronounced anisotropy in mechanical properties. Cooling of the previously deposited material and the low thermal mass of the new material result in inadequate reheating of the surface of the underlying layer. This leads to reduced molecular mobility and, consequently, weak interlayer adhesion. As a result, the mechanical strength in the build direction (Z-axis) is significantly lower than in the manufacturing plane [2]. To overcome this limitation, several approaches have been developed to elevate the temperature in the interlayer bonding zone. The most common approach is the use of heated build chambers to maintain a higher ambient temperature [3]. Other methods include heating via hot air [4], infrared radiation [5], microwaves [6], or contact-based surface heaters [7].

Building on previous feasibility studies that demonstrated the benefits of laser-based preheating — such as improved mechanical properties and reduced porosity [8] — a new experimental setup is realized in this work. It provides various laser intensity profiles, enabling direction-dependent preheating of the extruded strands. The aim of this study is to evaluate the effect of different laser intensity profiles, in combination with controlled part cooling, on mechanical performance with a focus on interlayer tensile strength. The results provide insights into optimizing thermal conditions during printing to overcome anisotropy and improve layer bonding in FLM components.

2. Experimental setup and methodology

2.1. Setup configuration

The experimental setup is based on a modified FLM printer (E3D Motion System with ToolChanger), equipped with an individually designed print head that integrates a laser-assisted preheating module. To minimize moving mass and improve dynamic stability, a Bowden extrusion system was implemented, relocating the filament feed motor to the printer frame. Due to the compact and enclosed design of the hotend assembly, a conventional part cooling fan was omitted. Instead, cooling is achieved via directed compressed air jets, which enables adequate thermal management during the deposition process.

Figure 1 (a) shows the modified printhead equipped with laser preheating and compressed air jets for part cooling. Figure 1 (b) schematically shows the allocation of the preheating and the part cooling area around the deposition area of the molten plastic. Toolpath generation and G-code creation are implemented via a custom MATLAB script, allowing precise control of the leaser preheating, synchronized with the extrusion trajectory.

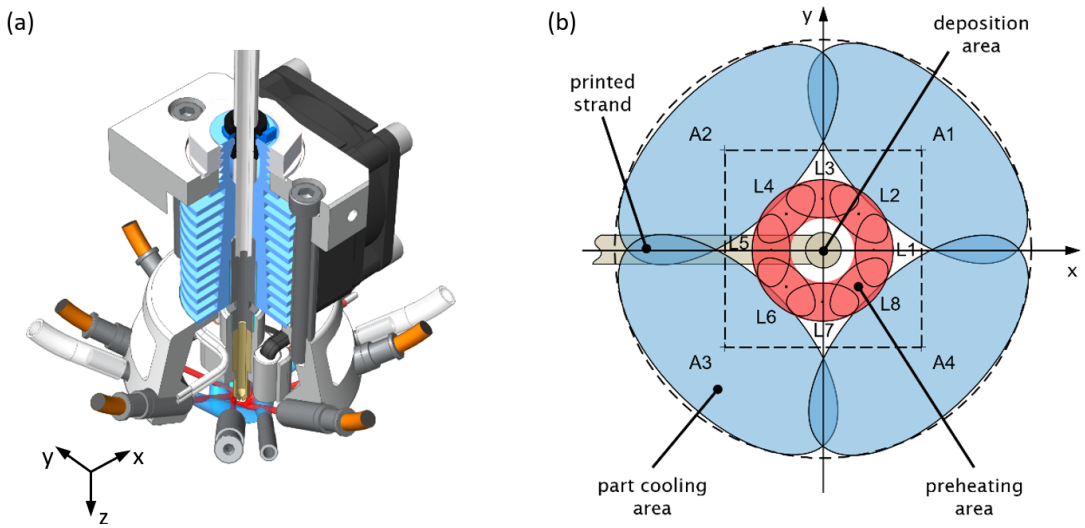

Fig. 1. (a) printhead equipped with eight collimator optics for laser preheating and four air jets for part cooling (b) allocation of the preheating and the part cooling area around the deposition area of the plastic filament.

2.2. Laser preheating module

The laser preheating module consists of eight collimated beams arranged concentrically around the nozzle. Each beam is generated by a fiber-coupled diode laser (λ = 450 nm), with the fiber glued in a custom ferrule that is directly mounted to a collimation lens, providing 1 mm beam diameter. Due to the oblique incidence on the part, the irradiated spots are elliptical. The eight spots superimpose to form an almost continuous ring-shaped heating zone around the extrusion nozzle.

To allow flexible control of the lasers, a custom firmware plugin was developed for the printer's control board (Duet3D Duet 3 6HC with SBC). This extension enables independent power modulation of each laser via embedded G-code commands, using a combination of trigger signals and power-level definitions. This setup facilitates dynamic intensity shaping along the print direction and allows generation of different intensity profiles such as spot, sickle, and ring distributions. Figure 2 (a) illustrates an example of the resulting laser intensity distribution using a power configuration of [80 %, 100 %, 80 %] computed for 10 W total laser output. That means laser 1 (L1) is powered with 100 % (3.8 W) and the lasers besides (L2 and L8) with 80 % (3.1 W) of the 10 W total laser power.

2.3. Cooling system

To ensure dimensional stability of the printed parts and prevent overheating of adjacent material zones, a cooling ring is implemented concentrically to the laser preheating module instead of a fan. The ring consists of four air jets, each delivering a directed stream of compressed air. Figure 2 (b) shows the airflow velocity distribution at the processing plane, measured with a wire anemometer, for the set value of v_F = 2 m/s airflow velocity of each nozzle (A1 – A4).

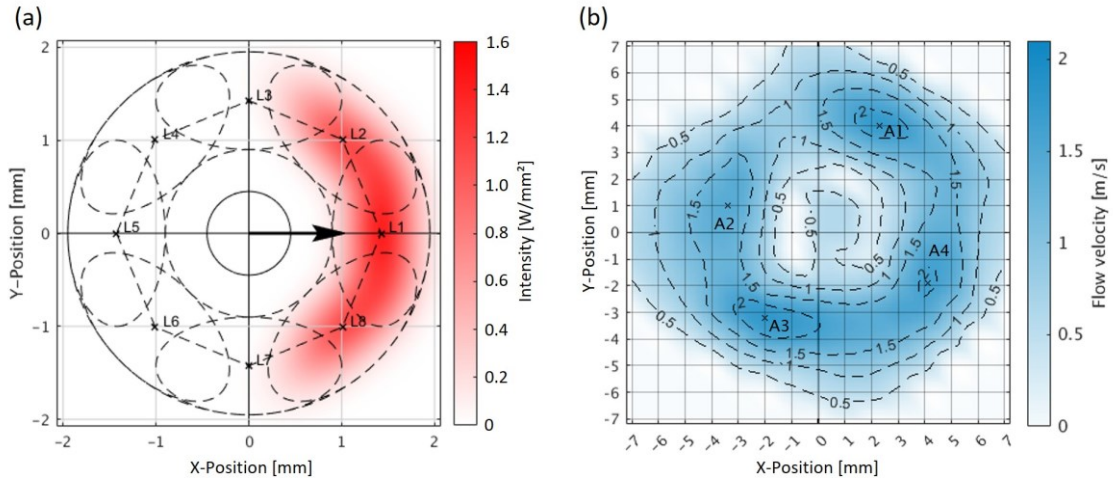

Fig. 2. (a) computed laser intensity distribution in printing direction using a power configuration of [80 %, 100 %, 80 %] at 10 W total laser power output. (b) measured airflow velocity distribution at the processing plane at the set value of v_F = 2 m/s at each nozzle

2.4. Specimen geometry and mechanical testing

Figure 3 (a) shows a drawing of the test specimen geometry, while figure 3 (b) displays the produced test specimens: The 75 mm long profiles were printed and then sectioned into five 5 mm thick specimens for tensile testing. A “hourglass”-shaped geometry is used instead of the standard tensile test geometry. This significantly shortens print time compared to vertically printed tensile test geometry (2 h vs 12 h), enabling higher throughput and thus more parameters studied in experimental series. Moreover, the hourglass geometry promotes failure at its narrowest section, which is placed between printed layers, making the geometry particularly suitable for evaluating interlayer-bonding.

Tensile testing of five specimens per parameter setting was performed in accordance with the general principles of DIN EN ISO 527-2 for tensile testing of plastics with 25 mm/min crosshead speed. Since the specimen geometry deviates from the standard geometry, the results discussed in this work refer to the maximum tensile stress σ_{HG} rather than the ultimate tensile strength as defined in DIN EN ISO 527-2. This distinction is made to clearly separate the results from standardized test values, emphasizing the focus on interlayer bonding under the given test conditions.

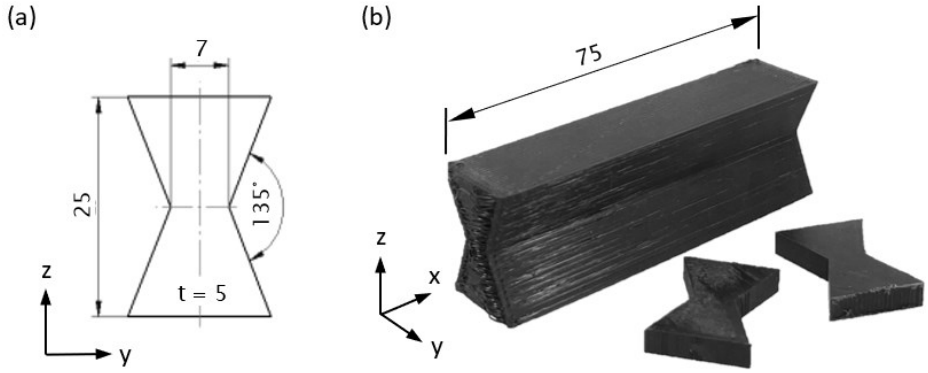

Fig. 3. (a) schematic of hourglass-shaped specimen geometry used for interlayer adhesion testing. (b) printed profile from which 5 mm thick test specimens were extracted.

2.5. Printing parameters

All specimens were fabricated using PLA (Prusament, Color Jet Black), a commercially available filament known for its good printability. The printing parameters are based on the “0.15 mm QUALITY” profile for the Prusa i3 MK3S printer, ensuring compatibility with standard slicing setups. The specimens were printed using 100 % infill density in a back-and-forth pattern along the x-axis with an offset of Δy = 0.45 mm between the strands. This was chosen to focus on the analysis of interlayer bonding effects rather than infill-related ones.

Table 1 shows the process parameters used for printing. The printing speed was kept constant at 80 mm/s. The part cooling was varied with three different airflow velocities v_F (2 m/s, 5 m/s, and 8 m/s). Printing with less cooling is not possible, as the parts become geometrically unstable. To evaluate the influence of thermal preheating, three different laser intensity distributions — spot, sickle, and ring — were implemented by selectively activating different combinations of the eight laser modules (L1 – L8). Within a range of 0 W to 6 W per laser, all active lasers operated at the same power level. The laser intensity distribution was dynamically aligned with the x-feed direction during printing. All lasers were deactivated during deceleration phases at turning points of the toolpath to prevent localized overheating due to reduced feed rate.

Table 1. Process parameters for investigation of the interlayer bonding and the influence of laser preheating and part cooling.

Intensity distribution (positive v_x):	spot	sickle	ring
	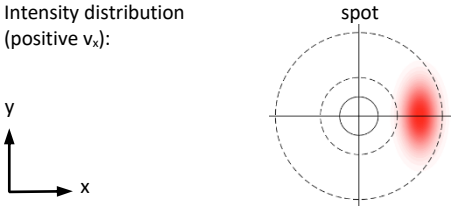		
Number of active lasers	1	3	8
positive v_x	L1	L1, L2, L4,	L1, L2, L3, L4, L5, L6, L7, L8
negative v_x	L5	L5, L6, L8	L1, L2, L3, L4, L5, L6, L7, L8
Laser power:		0 W to 6 W for each laser	
Printing velocity:		80 mm/s	
Airflow velocity v_F	2 mm/s	5 mm/s	8 mm/s

3. Results

3.1. Single-spot laser intensity distribution

Figure 4 shows the maximum tensile stress σ_{HG} of parts printed without laser heating (0 W) and with the single-spot laser intensity distribution in dependence on the laser power for three different airflow velocities v_F of 8 mm/s (a), 5 mm/s (b), and 2 mm/s (c). Without any laser heating (P = 0 W), a σ_{HG} of 36 MPa is achieved for the lowest airflow velocity v_F of 2 mm/s (c). This is an almost two times higher σ_{HG} than for v_F = 8 mm/s (σ_{HG} = 18 MPa, a) or v_F = 5 mm/s (σ_{HG} = 19 MPa, b). For the highest airflow velocity of v_F = 8 mm/s (a), σ_{HG} increases steadily with rising laser power from 18 MPa (0 W) up to 28 MPa (6.0 W). For v_F = 5 mm/s (b), σ_{HG} increases from 19 MPa (0 W) to 26 MPa (4 W) and remains almost constant until 5.5 W laser power. Above 5.5 W, printing was not possible due to geometrical instability. For v_F = 2 mm/s (c), σ_{HG} increases from 36 MPa (0 W) to 48 MPa (3.5 W and 4 W). Exceeding 4 W laser power leads to decreasing σ_{HG} (42 MPa, 4.5 W and 5.0 W). Above 5.0 W, printing was not possible due to geometrical instability and thus an instable printing process.

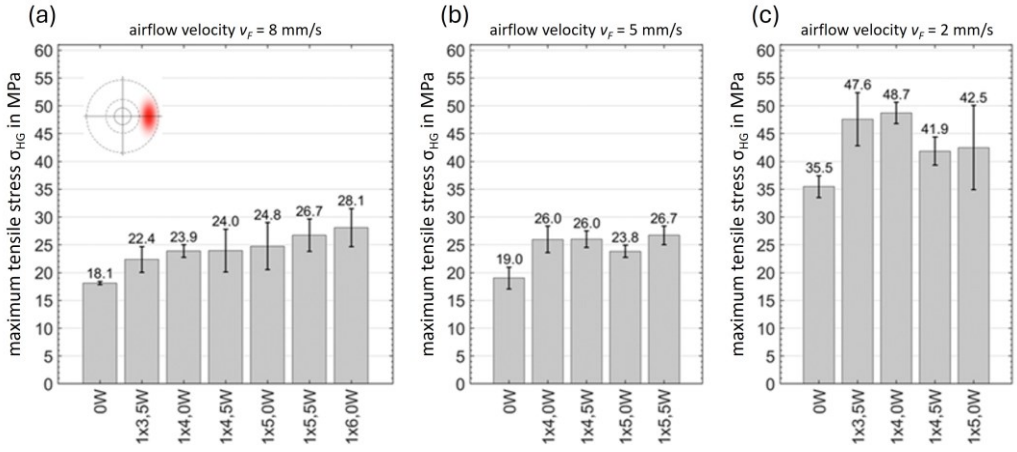

Fig. 4. maximum tensile stress σ_{HG} of PLA samples printed with spot-shaped laser intensity distribution under varying part cooling conditions (v_F = 8 mm/s (a), 5 mm/s (b), 2 mm/s (c)).

3.2. Sickle-shaped laser intensity distribution

Figure 5 shows the maximum tensile stress σ_{HG} for the sickle-shaped laser intensity distribution as a function of laser power (three lasers on) and the three different airflow velocities v_F. The σ_{HG} values without laser power (P = 0 W) are taken from figure 4 and are therefore identical. For a flow velocity v_F of 8 mm/s (Figure 5a), σ_{HG} increases from 18 MPa at 0 W to 29 MPa at 3x 3.0 W. Between 3x 3.0 W and 3x 4.5 W, σ_{HG} remains almost constant. Beyond 3x 4.5 W, the printing process became unstable.

For a v_F of 5 mm/s (Figure 5b), σ_{HG} increases to a plateau of 36 MPa in the range of 3x 3.0–4.0 W. At 3x 4.5 W, σ_{HG} decreases to 30 MPa and beyond this laser power, the process became unstable. For v_F = 2 mm/s (Figure 5c), σ_{HG} rises from 36 MPa (0 W) to a maximum of 50 MPa at 3x 2.5 W. A further increase in laser power leads to a decrease of σ_{HG} to 37 MPa at both 3x 3.0 W and 3x 3.5 W, finally resulting in an unstable printing process beyond 3x 3.5 W.

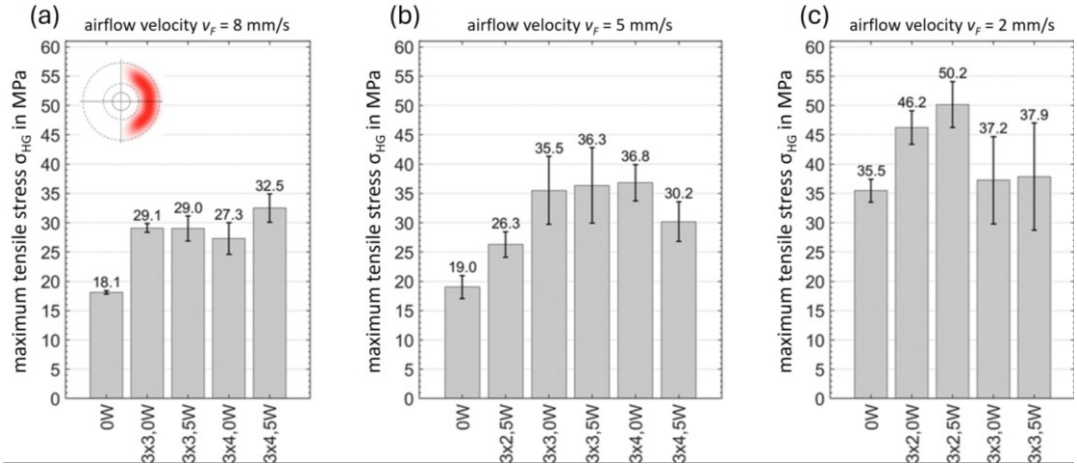

Fig. 5. maximum tensile stress σ_{HG} of PLA samples printed with sickle-shaped laser intensity distribution under varying part cooling conditions (v_F = 8 mm/s (a), 5 mm/s (b), 2 mm/s (c)).

3.3. Ring-shaped laser intensity distribution

Figure 6 shows the maximum tensile stress σ_{HG} for the ring-shaped laser intensity distribution in dependence on the laser power (all eight lasers on) and the three different airflow velocities v_F. For v_F = 8 mm/s (a), σ_{HG} increases from 18 MPa (0 W) to a maximum of 39 MPa (8x 2 W). A further increase in laser power leads to decreasing σ_{HG} (8x 2.5–3.0 W) and an instable process if exceeding 8x 3 W. For v_F = 5 mm/s (b), σ_{HG} increases steadily with rising laser power from 19 MPa (0 W) up to 47 MPa (8x 2.5 W). Increasing the laser power further leads to a halving of σ_{HG} (23 MPa, 8x 3.0 W), almost down to the value without laser heating, and an instable process if exceeding 8x 3.0 W. For v_F = 2 mm/s (c), σ_{HG} increases from 36 MPa (0 W) to a maximum of 51 MPa (8x 1.0 W). A further increase leads to a reduction of σ_{HG} (40 MPa and 36 MPa for 8x 1.5–2 W) and an instable process if exceeding 8x 2 W.

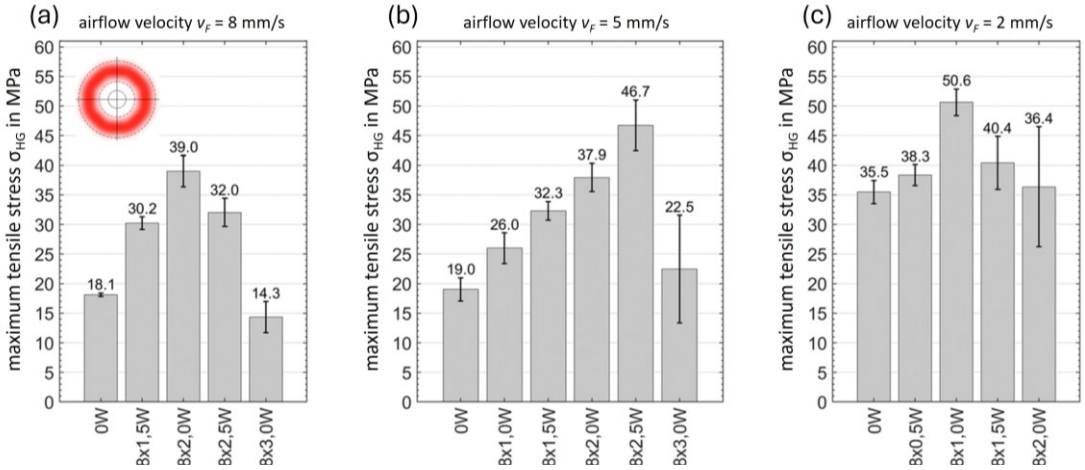

Fig. 6. maximum tensile stress σ_{HG} of PLA samples printed with ring-shaped laser intensity distribution under varying part cooling conditions (v_F = 8 mm/s (a), 5 mm/s (b), 2 mm/s (c)).

3.4. Comparison of single-spot, sickle-, and ring-shaped laser intensity distribution

Compared to no laser assistance (σ_{HG} = 36 MPa, v_F = 2 m/s, 0 W), the maximum σ_{HG} is increased by approx. 40 % up to approx. 50 MPa for all three laser intensity distributions (Figure 4c, 5c, 6c). Despite not reaching this global maximum for higher v_F, an increase of σ_{HG} due to laser preheating is observed for v_F = 5 m/s and v_F = 8 m/s as well: The σ_{HG} of 18 MPa (8 m/s, a) and 19 MPa (5 m/s, b) achieved without laser assistance is more than doubled (+ > 100 %) using the ring-shaped (v_F = 5 m/s and 8 m/s, Figure 6a, b) and sickle-shaped (v_F = 5 m/s, Figure 5b) intensity profiles. For v_F = 5 m/s and a ring-shaped distribution, the overall largest improvement of 145 % is achieved (Figure 6b). For the single-spot (Figure 4a, b) and the sickle-shaped profiles at v_F = 8 m/s (Figure 5b), σ_{HG} is still increased by 50 % compared to σ_{HG} without laser heating.

Notably, only the ring-shaped intensity enables the surpassing of the without-laser maximum σ_{HG} (36 MPa, v_F = 2 m/s, 0 W) for all three flow velocities v_F.

Analyzing the general dependency of laser power and airflow velocity over all three laser intensity distributions shows, that the stronger the cooling (i.e., higher airflow velocity v_F), the greater the laser power required to achieve an improvement. Simultaneously, the maximum allowable laser power before geometric instability occurs increases with increasing flow velocity v_F. The use of multiple laser diodes (e.g., sickle- or ring-shaped profiles) leads to earlier onset of instability at lower power levels per diode.

4. Discussion

The analysis of the maximum tensile stress σ_{HG} reveals that, without laser irradiation, the highest mechanical strength is achieved for v_F = 2 m/s, representing the minimal possible cooling condition and thus the highest temperature at the deposition area possible without laser heating. The increase of strength with higher temperature (caused by less cooling) is consistent with findings in laser plastic welding [9, 10] and Fused Layer Modeling [11], where elevated temperatures promote improved bonding between layers. Utilizing the additional heat input of laser-based preheating, the maximum tensile stress σ_{HG} attainable in build direction can be increased by approx. 40 % compared to no-laser heating, while maintaining geometrical stability due to the only localized heat input.

The dependency of mechanical strength and process instability on laser power and cooling conditions shows, that laser power must be well balanced in dependence on the cooling conditions. This enables maximum mechanical strength while maintaining process stability. The finding that higher laser powers are required under increased cooling — caused by higher airflow velocities v_F — is consistent with expectations based on thermal energy balance considerations.

Regarding the target application —printing of large components with long layer times — the strong localized cooling due to forced convection by a fast airflow will superimpose with the slower conductive and natural convective cooling, which becomes increasingly significant at prolonged layer deposition times. Since balancing laser power in dependence on the cooling conditions is crucial for achieving maximum mechanical strength while maintaining process stability, temperature monitoring and closed-loop laser power control are recommended to allow full exploitation of the +40 % strength improvement demonstrated in build direction.

5. Conclusion and outlook

Additive manufacturing via material extrusion often suffers from insufficient interlayer bonding, leading to reduced mechanical performance and pronounced anisotropy in printed parts. This study confirms the potential of laser-assisted preheating to enhance the interlayer bonding in material extrusion AM: The maximum strength achievable without laser preheating can be increased by more than 40 %, while maintaining a stable printing process.

To be able to utilize the potential of laser-assisted preheating, the temperature field in the deposition zone will be quantified using in-situ diagnostics (e.g., thermal imaging) in future work. Thus, the laser power could be controlled regarding ideal temperature for layer bonding – compensating the effects of part geometry, cooling conditions and printing facility (e.g. printhead design and filament feed) – while maintaining geometrical stability of the entire part.

Acknowledgements

The results presented in this publication were obtained within the project 'LE-FLM', which is funded under the Central Innovation Programme for SMEs (ZIM KK5608901SYM) by the Federal Ministry for Economic Affairs and Climate Action on the basis of a resolution of the German Bundestag.

References

[1] Sculpteo: The State of 3D Printing (2022 Edition), www.sculpteo.com, Retrieved on June 11, 2025 from https://www.sculpteo.com/en/ebooks/state-of-3d-printing-report-2022/

[2] Reindl, T; Meisner, D.; Hierl, S.: Benchmarking of plastic-based Additive Manufacturing Processes. In: RTe Journal, 2023. doi:10.58134/fh-aachen-rte_2023_002

[3] Additive Fertigungsverfahren Gestaltungsempfehlungen für die Bauteilfertigung mit Materialextrusionsverfahren, VDI 3405 Blatt 3.4, VDI Verein Deutscher Ingenieure e.V., Berlin, Jul. 2019.

[4] Prajapati, H.; Salvi, S. S.; Ravoori, D.; Qasaimeh, M.; Adnan, A. and Jain,A.: Improved print quality in fused filament fabrication through localized dispensing of hot air around the deposited filament, Additive Manufacturing, vol. 40, p. 101917, 2021. doi: 10.1016/j.addma.2021.101917

[5] Kishore, V.; Ajinjeru, C., Nycz, A.; Post, B.; Lindahl, J.; Kunc, V. and Duty, C.: Infrared preheating to improve interlayer strength of big area additive manufacturing (BAAM) components," Additive Manufacturing, vol. 14, pp. 7–12, 2017. doi: 10.1016/j.addma.2016.11.008

[6] Andreu, A.; Kim, S.; Dittus, J.; Friedmann, M.; Fleischer J. and Yoon, Y.-J.: Hybrid material extrusion 3D printing to strengthen interlayer adhesion through hot rolling, Additive Manufacturing, vol. 55, p. 102773, 2022. doi: 10.1016/j.addma.2022.102773

[7] Andreas, J. W. H.; Popp, U.; Pfotzer, L.; Okolo, B.; and Tran, M.T.: 3D-Druckvorrichtung, DE102015111504 (A1), DE DE201510111504 20150715, Jan 19, 2017.

[8] Meisner, D.; Forstner, L.; Kaftiranis, N.; Hierl S.: Investigation of process improvements through laser preheating in extrusion-based additive manufacturing process. In: Lasers in Manufacturing Conference, München, 2023.

[9] Schmailzl, A: Festigkeits- und zeitoptimierte Prozessführung beim quasi-simultanen Laser-Durchstrahlschweißen. In: FAU Studien aus dem Maschinenbau Band 406, Erlangen: FAU University Press, 2022. doi: 10.25593/978-3-96147-584-1

[10] Maiwald, F.; Kroth, L.; Geiger, R.; Schmitt, B.; Hierl, S.; Schmidt, M.: Laser welding of polymer foils with spatially adapted intensity distributions. In: JOINING PLASTICS 19 No. 1, 2025, ISSN: 1864-3450. doi: 10.53192/JP20250146

[11] Seppala, J. E.; Hoon Han, S.; Hillgartner, K. E.; Davis, C. S.; Migler, K. B.: Weld formation during material extrusion additive manufacturing. In: Soft matter 13 (2017), Nr. 38, S. 6761–6769. doi:10.1039/c7sm00950j